Actas de las XXXVI Jornadas de Automática, 2 - 4 de septiembre de 2015. Bilbao
ISBN 978-84-15914-12-9

Torque distribution strategy for a four In-wheel fully electric car.

Ezequiel Debada
Department of Systems Engineering and Automatic Control, University of Seville, ezequielgd@us.es

David Marcos, Carlos Montero, Eduardo F. Camacho, Carlos Bordons, Miguel A. Ridao
Department of Systems Engineering and Automatic Control, University of Seville. Spain.
{dmarcos, cmontero1, efcamacho, bordons, miguelridao}@us.es

Abstract

Electromobility promises to have a strong impact in several aspects of our life: introducing new means of transport concepts, proposing new business models and allowing to create new vehicle configurations impossible with traditional combustion engines. Regarding the latter, this paper presents a novel torque distribution strategy for a 4 in-wheel electric vehicle which aims to reduce the total longitudinal slip. The control strategy is designed off-line supported by a simulator and tested both in simulation (with a different model from the used for designing) as well as on a real sized prototype. The results show that the total longitudinal slip is successfully reduced after applying the control strategy and additionally, the radius described by the vehicle while cornering is slightly closer to the theoretical Ackerman radius.

KeyWords: Torque Distribution, Torque Vectoring, In-wheel electric motors.

1 Introduction

The important energy implications of hybrid and electric vehicles have been extensively discussed [7, 1], and they are considered key points regarding several environmental problems' solution. The interest in the development of these vehicles is growing and that, together with the greater demand, encourages the industry to produce new kinds of hybrid and Electric Vehicles (EVs) in mass. However, the EVs convenience is not limited to the energetic aspects. The own nature of electric motors presents several advantages over internal combustion engines [9], such as:

- Faster torque response.
- Measurable output torque through motor current.
- In-wheel configuration.
- Regenerative breaking.
- Less consumption.
- New control possibilities.

These advantages motivate the existence of research trends for developing traction control methods. In that sense, the concept of electronic differential was proposed in [9, 19], and more recently, its use for enhancing the vehicle behavior and the safety under certain circumstances (Torque Vectoring (TV) control) is being studied [4] .

Several approaches have been used to face this problem [8, 17, 3, 6]. De novellis *et al.* in [13, 5] classify them in four groups, depending on the used strategy:

- Minimization of the overall input motor power.
- Minimization of the standard deviation of longitudinal tire slip with respect to the average slip of the four wheels.
- Minimization of the total longitudinal slip power loss.
- Minimization of the average combined tire force coefficient.

They also use a car simulator to compare controllers with different criteria. Despite not having a widely accepted approach, they conclude that the *total longitudinal slip power loss* option carries several advantages compared with the others. In that sense, this paper adopts an analogous *total longitudinal slip reduction* criteria.

The main contribution of this work consists of an adaptive torque allocation strategy designed offline which reduces the total longitudinal slip. The control strategy design makes use of a vehicle dynamic model tuned with a real prototype named FOX [12], and subsequently it is tested over the real vehicle and a more accurate and validated model [12, 18].

The present paper is organized as follows. The real vehicle is described in Section 2. The dynamic

ISBN 978-84-15914-12-9

Figura 1: Fox vehicle.

model is exposed in Section 3. The controller design methodology is presented in Section 4. Section 5 describes the tests whose results are shown and discussed afterwards in Section 6. Finally, Section 7 includes some conclusions and future research threads.

2 Vehicle Description

The FOX vehicle is based on the chassis of the Silver Car S2 racing car. It was slightly modified for the best fitting of the new elements and for adding a second seat. The bodywork is the same as the original S2 car. Figure 1 shows the vehicle completely mounted. The main components of the vehicle are:

Motors

The car is powered by four brushless hub motors, 7 kW power each, driven by commercial converters. The characterization of the motors, provided by the manufacturer, is shown in Fig. 2.

Batteries

The power source is composed by six packs of four cells of LiFeMnPO4 batteries. Their main specifications are shown in table 1 (data supplied by the manufacturer). These batteries are controlled by a commercial Battery Management and Monitoring Systems (BMS).

Sensors

Several sensors of different types have been installed in the car, with two aims: set the parameters of the model and, in the end of the modelling process, compare the results with the real case, and validate the model, and measure some parameters to obtain the state of the vehicle and the signals set by the driver, so the controller actuates consequently.

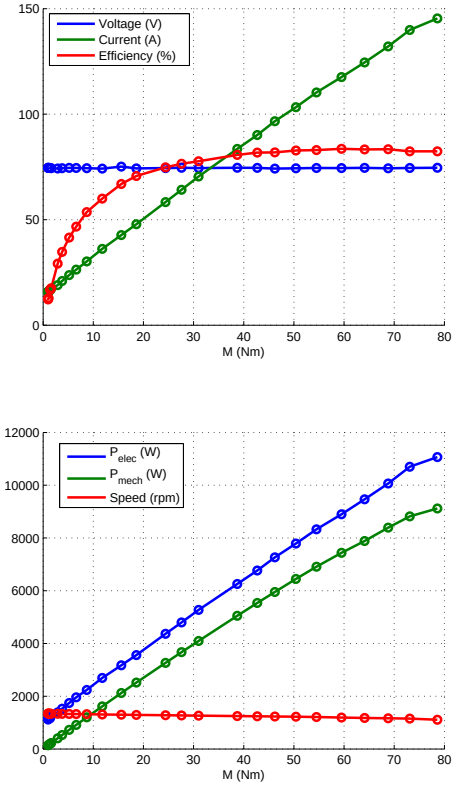

Figura 2: In-wheel motor characterization.

- Inertial Measure Unit (IMU): this device measures the linear and angular accelerations in the three axis, as well as the magnetic field. It also include a Global Positioning System (GPS), that will add an external position measurement. The IMU installed in the vehicle is the model 3DM-GX3-35, from the manufacturer Microstrain.
- Accelerator: 0 to 5 volts signal, proportional to the pedal position.
- Brake pedal sensor: potentiometer. Nominal resistance: 10 kω. Accuracy: 0.034%.
- Steering Wheel angle sensor.

Tabla 1: Specifications of the batteries.

Nominal Voltage	12.8V (4x3.2 V)
Nominal Capacity	100 Ah
Operation Voltage Range	11.2 to 14.4V
Weight	12.9 kg
Dimension	270x140x241 mm
Max Charging Current	3C
Max Discharge Current	3C (cont.) / 10C (pul.)
Cycle Life	>2000
Operating Temperature	20 to 65 ^oC
Self Discharge Rate	<3% monthly

ISBN 978-84-15914-12-9

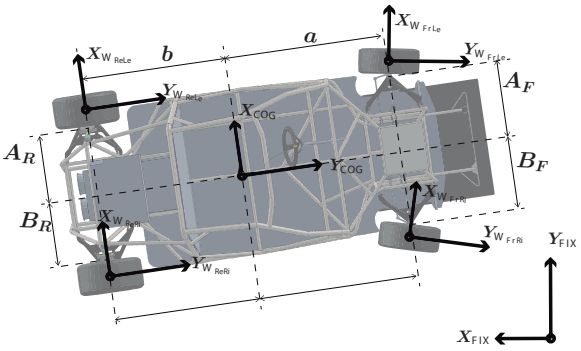

Figura 3: Coordinate Systems

3 Modeling

The control strategy detailed in Section 4 uses a simplified vehicle dynamic model that is presented in this Section.

Model architecture

The model consists of four wheels and one vehicle body rigidly connected where only the front wheels can be steered. As mentioned before, the torque requested by the driver can be applied over the four wheels and its distribution can change dynamically.

Different coordinates systems are considered (Figure 3): an inertial coordinate system defined as a fixed system, the center of gravity coordinate system with its origin in the center of gravity of the vehicle and finally, one coordinate system for each wheel.

Vehicle kinematics

The kinematic equations referred to the Center of Gravity (CoG) and the fixed coordinate system are formulated as follows [11].

$$\overrightarrow{v}_{\mathrm{COG}_{\mathrm{COG}}} = \begin{bmatrix} v_{\mathrm{COG}}\cos(\beta) \\ v_{\mathrm{COG}}\sin(\beta) \end{bmatrix} \tag{1}$$

$$\overrightarrow{v}_{\mathrm{COG}_{\mathrm{FIX}}} = \begin{bmatrix} v_{\mathrm{COG}}\cos(\beta+\psi) \\ v_{\mathrm{COG}}\sin(\beta+\psi) \end{bmatrix} \tag{2}$$

$$\overrightarrow{a}_{\mathrm{COG}_{\mathrm{FIX}}} = v_{\mathrm{COG}}(\dot{\beta}+\dot{\psi}) \begin{bmatrix} -\sin(\beta+\psi) \\ \cos(\beta+\psi) \end{bmatrix} + + \dot{v}_{\mathrm{COG}} \begin{bmatrix} \cos(\beta+\psi) \\ \sin(\beta+\psi) \end{bmatrix} \tag{3}$$

$$\overrightarrow{a}_{\mathrm{COG}_{\mathrm{COG}}} = v_{\mathrm{COG}}(\dot{\beta}+\dot{\psi}) \begin{bmatrix} -\sin\beta \\ \cos\beta \end{bmatrix} + + \dot{v}_{\mathrm{COG}} \begin{bmatrix} \cos\beta \\ \sin\beta \end{bmatrix} \tag{4}$$

Where v_{COG} is the vehicle speed, β is the side slip angle (the angle between $\overrightarrow{v}_{\mathrm{COG}}$ and $\overrightarrow{x}_{\mathrm{COG}}$), and ψ is the yaw angle (Figure 4).

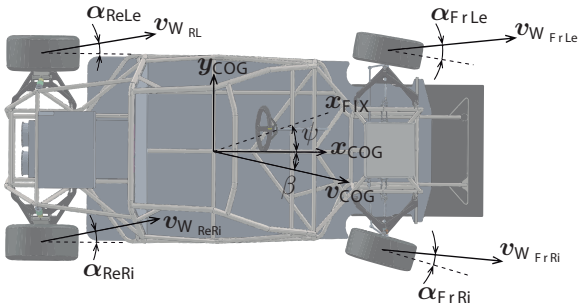

Figura 4: Velocities

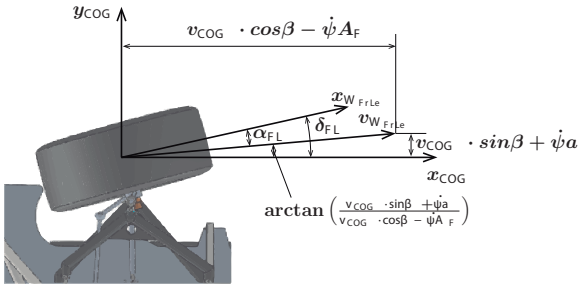

Figura 5: Slip angle

Tire kinematics

Wheel velocities are calculated following Equations 5-8 for small values of β.

$$\overrightarrow{v}_{\mathrm{W}_{FL_{\mathrm{COG}}}} = \begin{bmatrix} v_{\mathrm{COG}}\cos\beta - \dot{\psi}A_{\mathrm{F}} \\ v_{\mathrm{COG}}\sin\beta + \dot{\psi}a \end{bmatrix} \tag{5}$$

$$\overrightarrow{v}_{\mathrm{W}_{FR_{\mathrm{COG}}}} = \begin{bmatrix} v_{\mathrm{COG}}\cos\beta + \dot{\psi}B_{\mathrm{F}} \\ v_{\mathrm{COG}}\sin\beta + \dot{\psi}a \end{bmatrix} \tag{6}$$

$$\overrightarrow{v}_{\mathrm{W}_{RL_{\mathrm{COG}}}} = \begin{bmatrix} v_{\mathrm{COG}}\cos\beta - \dot{\psi}A_{\mathrm{R}} \\ v_{\mathrm{COG}}\sin\beta + \dot{\psi}b \end{bmatrix} \tag{7}$$

$$\overrightarrow{v}_{\mathrm{W}_{FL_{\mathrm{COG}}}} = \begin{bmatrix} v_{\mathrm{COG}}\cos\beta + \dot{\psi}B_{\mathrm{R}} \\ v_{\mathrm{COG}}\sin\beta + \dot{\psi}b \end{bmatrix} \tag{8}$$

Where A_{F}, A_{R}, B_{F}, B_{R} a and b correspond to the car dimensions as illustrated in Figure 3.

Figure 4 shows all the velocities described in this section as well as the side slip angles (α's) that are calculated using each wheel velocity vector [16, p. 316] as Figure 5 and Equation 12 show.

$$\alpha_{\mathrm{FL}} = \delta_{\mathrm{W}_{\mathrm{FL}}} - \arctan\frac{v_{\mathrm{COG}}\sin\beta + \dot{\psi}a}{v_{\mathrm{COG}}\cos\beta - \dot{\psi}A_{\mathrm{F}}} \tag{9}$$

$$\alpha_{\mathrm{FR}} = \delta_{\mathrm{W}_{\mathrm{FR}}} - \arctan\frac{v_{\mathrm{COG}}\sin\beta + \dot{\psi}a}{v_{\mathrm{COG}}\cos\beta + \dot{\psi}B_{\mathrm{F}}} \tag{10}$$

$$\alpha_{\mathrm{RL}} = -\arctan\frac{v_{\mathrm{COG}}\sin\beta - \dot{\psi}b}{v_{\mathrm{COG}}\cos\beta - \dot{\psi}A_{\mathrm{R}}} \tag{11}$$

$$\alpha_{\mathrm{RR}} = -\arctan\frac{v_{\mathrm{COG}}\sin\beta - \dot{\psi}b}{v_{\mathrm{COG}}\cos\beta + \dot{\psi}B_{\mathrm{R}}} \tag{12}$$

ISBN 978-84-15914-12-9

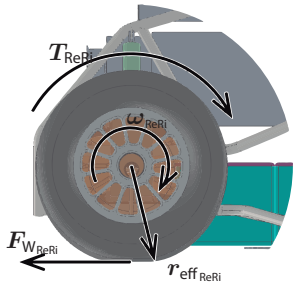

Figura 6: Tire dynamic balance

Wheel slip calculation

This work adopts Buckhardt formulation (Equations 13-14) to calculate the Longitudinal Slip (LS) and the Side Slip (SS) value [11, 16].

$$\text{LS} = \begin{cases} \frac{\omega r \cos\alpha - v_{\text{W}}}{v_{\text{W}}} & \text{if } \omega r \cos\alpha \leq v_{\text{W}} \\ \frac{\omega r \cos\alpha - v_{\text{W}}}{\omega r \cos\alpha} & \text{if } \omega r \cos\alpha \geq v_{\text{W}} \end{cases} \quad (13)$$

$$\text{SS} = \begin{cases} \frac{\omega r \sin\alpha}{v_{\text{W}}} & \text{if } \omega r \cos\alpha \leq v_{\text{W}} \\ \tan\alpha & \text{if } \omega r \cos\alpha \geq v_{\text{W}} \end{cases} \quad (14)$$

where ω is the angular velocity of the wheel and r is its radius.

Vehicle dynamics

The longitudinal/lateral force balance over the body of the vehicle and the equilibrium of moments on the tires are needed to calculate the accelerations.

Vehicle body dynamics

The force balance equations which allow to calculate the system accelerations are the next:

$$\dot{v}_{\text{COG}} = \frac{\cos\beta}{m}\left[\sum F_{\text{X}}\right] + \frac{\sin\beta}{m}\left[\sum F_{\text{Y}}\right] \quad (15)$$

$$\dot{\beta} = \frac{\cos\beta}{m v_{\text{COG}}}\sum F_{\text{Y}} - \frac{\sin\beta}{m v_{\text{COG}}}\sum F_{\text{X}} - \dot{\psi} \quad (16)$$

$$J_Z\ddot{\psi} = [F_{\text{Y}_{\text{FL}}} + F_{\text{Y}_{\text{FR}}}]\,a - [F_{\text{Y}_{\text{RL}}} + F_{\text{Y}_{\text{RR}}}]\,b + \\ + F_{\text{X}_{\text{FR}}}B_{\text{F}} - F_{\text{X}_{\text{FL}}}A_{\text{F}} + F_{\text{X}_{\text{RR}}}B_{\text{R}} - F_{\text{X}_{\text{RL}}}A_{\text{R}} \quad (17)$$

Where:

$$\sum F_{\text{X}} = \sum\left(F_{\text{W}_{\text{X}_{ij}}} - F_{\text{roll}_{ij}}\right) - F_{\text{aero}_{\text{x}}} \quad (18)$$

$$\sum F_{\text{Y}} = \sum F_{\text{W}_{\text{Y}_{ij}}} - F_{\text{aero}_{\text{y}}} \quad (19)$$

Tire dynamic balance

The forces experienced on each wheel are shown in Figure 6 and its dynamic balance corresponds to Equation 20:

$$I_{\text{W}}\dot{\omega} = T - r_{\text{eff}}F_{\text{W}} \quad (20)$$

where I_{W} is the moment of inertia of the wheel, $\dot{\omega}$ is the tire angular acceleration (rad/s^2), T is the torque applied (Nm), r_{eff} is the effective tire radius (m) and F_{W} is the force transmitted by the wheel (N).

Forces description

The different forces that act over the vehicle are gathered in this Section.

Aerodynamic force

The aerodynamic force [16, p. 97,p. 331] is calculated with Equation 21.

$$F_{\text{aero}} = C_{\text{ax}}S_{\text{front}}/2\rho_{\text{a}}v_{\text{x}}^2 \quad (21)$$

where F_{aero} is the aerodynamic resistance (N), C_{ax} is the aerodynamic resistance coefficient [10], S_{front} is the frontal area (m^2), ρ_{a} corresponds to the air density (kg/m^3) and v_{x} is the vehicle longitudinal velocity (m/s).

Friction forces

The friction model used in this work is the one proposed by Buckhardt in [2][16, P. 319]. It models the friction force as a static friction and approximates the tire characteristic through a linear relation with the vertical load in each wheel. Besides he splits it in two components for each wheel: one in the direction of v_{W} (F_{L}) and other one perpendicular to that (F_{S}).

The longitudinal and lateral friction coefficients are calculated through two auxiliary parameters S_{Res} and μ_{Res} (Equations 23-22).

$$\mu(S_{\text{Res}}) = c_1\left(1 - e^{-c_2 s_{\text{Res}}}\right) - c_3 S_{\text{Res}} \quad (22)$$

$$S_{\text{Res}} = \sqrt{\text{LS}^2 + \text{SS}^2} \quad (23)$$

Where coefficients c_1, c_2 y c_3 take different values according to the road conditions [16, p. 322].

Longitudinal and lateral friction coefficients are calculated as follows:

$$\mu_{\text{L}} = \mu_{\text{Res}}\frac{\text{LS}}{S_{\text{Res}}} \qquad \mu_{\text{S}} = \mu_{\text{Res}}\frac{\text{SS}}{S_{\text{Res}}} \quad (24)$$

With that information, the forces produced in the tires are calculated with Equation 25

$$\sqrt{F_{\text{W}_{\text{L}}}^2 + F_{\text{W}_{\text{S}}}^2} \leq \mu_{\text{Res}}F_{\text{Z}} \quad (25)$$

Roll resistance

Roll resistance is calculated with Equation 26.

$$F_{\text{roll}} = f_{\text{roll}} \sum_{i=\{\text{Fr,Re}\}} \sum_{j=\{\text{Le,Ri}\}} (F_{\text{Z}_{ij}}) \quad (26)$$

Where f_{roll} is the friction coefficient [15].

ISBN 978-84-15914-12-9

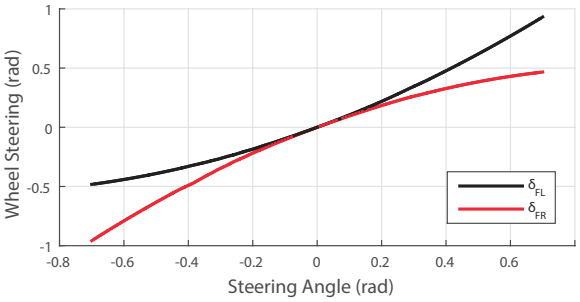

Figura 7: Experimental steering angles relation obtained from Fox.

Vertical load

Neglecting suspension effects, each vertical force can be calculated separately with Equations 27, 28, 29 and 30 [11].

$$F_{Z_{FL}} = m\left(\frac{b}{a+b}g - \frac{h_{COG}}{a+b}a_{X_{Ch}}\right)\cdot \cdot\left[\frac{1}{2} - \frac{h_{COG}a_{Y_{Ch}}}{(A_F+B_F)g}\right] \quad (27)$$

$$F_{Z_{FR}} = m\left(\frac{b}{a+b}g - \frac{h_{COG}}{a+b}a_{X_{Ch}}\right)\cdot \cdot\left[\frac{1}{2} + \frac{h_{COG}a_{Y_{Ch}}}{(A_F+B_F)g}\right] \quad (28)$$

$$F_{Z_{RR}} = m\left(\frac{a}{a+b}g + \frac{h_{COG}}{a+b}a_{X_{Ch}}\right)\cdot \cdot\left[\frac{1}{2} - \frac{h_{COG}a_{Y_{Ch}}}{(A_R+B_R)g}\right] \quad (29)$$

$$F_{Z_{RL}} = m\left(\frac{a}{a+b}g + \frac{h_{COG}}{a+b}a_{X_{Ch}}\right)\cdot \cdot\left[\frac{1}{2} + \frac{h_{COG}a_{Y_{Ch}}}{(A_R+B_R)g}\right] \quad (30)$$

Steering geometry

The relation between the steering and the two wheels steering angles has been obtained experimentally from Fox. Figure 7 shows the resulting relation.

Validation

After tunning the model parameters, the comparison between the model behavior and the real one reports an enough grade of similarity to consider the model suitable for being used in the control design stage. Figure 8 shows the comparison of the accelerations registered during a real test and the ones reported by the simulation using the real input signals.

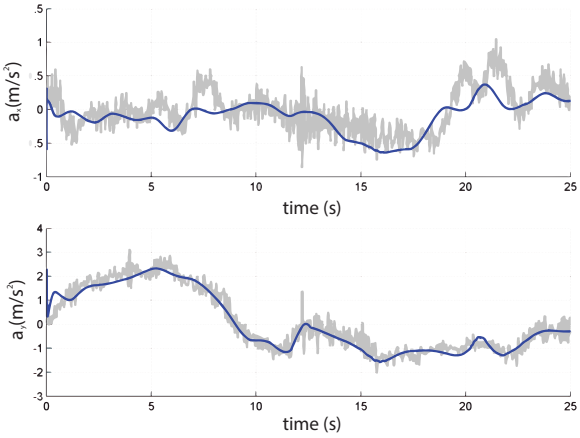

Figura 8: Accelerations comparison between the real signal measured (gray) and the reported by the simulation (blue)

4 Torque Distribution

The torque distribution strategy consists of the next steps. First, a set of simulation scenarios is defined by selecting the vehicle steering angle and speed for each of them. In every simulation, an objective function value under different torque distribution conditions is measured and among all those values, the minimum is considered the optimal. Those points are subsequently processed to obtain a continuous and smooth evolution that relates driving conditions (steering angle and speed) to the optimal torque distribution.

Problem formalization and nomenclature

Given a certain torque T requested by the driver and a set of external variables Ω, the best torque distribution Δ which minimizes the total longitudinal slip ratio LS is calculated.

$$\Delta = argmin_{\Delta}\sum \mathrm{LS}(T,\Omega) \quad (31)$$

Where the torque demanded T is given by the position of the accelerator and Ω comprises the car speed v_c and the steering angle α ($\Omega = \{v_c, \alpha\}$). The torque distribution is defined by the value of the following parameters:

$$\Delta = \left\{ \begin{array}{ccc} \delta_{Fr} & \delta_{FrLe} & \delta_{ReLe} \end{array} \right\} \quad (32)$$

where:

- $\delta_{Fr} \in (0,1)$ represents the longitudinal axis torque distribution.
- $\delta_{FrLe} \in (0,1)$ represents the lateral torque balance on the front axle.
- $\delta_{ReLe} \in (0,1)$ represents the lateral torque balance on the rear axle.

ISBN 978-84-15914-12-9

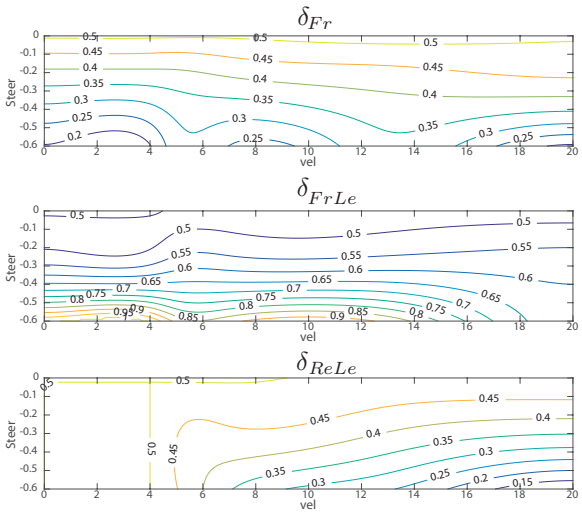

Figura 9: Torque distribution

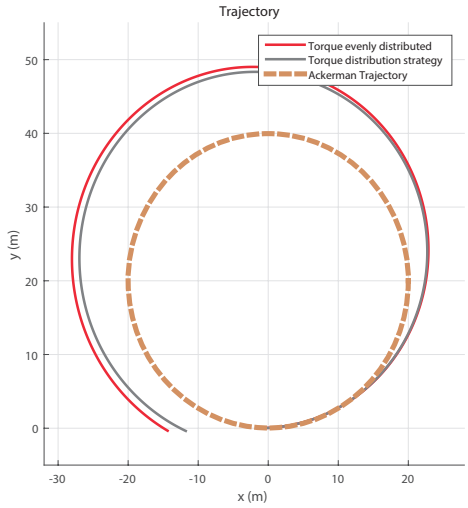

Figura 10: Red: Torque evenly distributed, Gray: Torque distribution according to control

Consequently, the torque allocated in each wheel is expressed by:

$$T_{\mathrm{FrLe}} = T\delta_{\mathrm{Fr}}\delta_{\mathrm{FrLe}} \quad (33)$$

$$T_{\mathrm{FrRi}} = T\delta_{\mathrm{Fr}}(1-\delta_{\mathrm{FrLe}}) \quad (34)$$

$$T_{\mathrm{ReLe}} = T(1-\delta_{\mathrm{Fr}})\delta_{\mathrm{ReLe}} \quad (35)$$

$$T_{\mathrm{ReRi}} = T(1-\delta_{\mathrm{Fr}})(1-\delta_{\mathrm{FrLe}}) \quad (36)$$

Where the subscripts Fr, Re, Le and Ri denote the front, rear, left and right wheels respectively.

Control design

The parameters range considered to generate the set of simulations commented at the beginning of this section are:

- $v \in (0, 20]$ m/s
- $\alpha \in [-\alpha_{\max}, 0)$. Where $\alpha_{\max}$ is the maximum steering angle and only negative values are considered since a symmetric behavior is assumed.
- $\delta_i \in (0, 1) \forall i = \{\mathrm{Fr}, \mathrm{FrLe}, \mathrm{ReLe}\}$.

For each simulation scenario defined by a pair steering angle-speed, every combination of torque distribution is tested. The one resulting in the minimum total longitudinal slip in steady state is considered the optimal.

By processing the resulting points, three tables describing the torque distribution strategy are obtained (one for each component of Δ). A possible representation of such tables is shown in Figure 9 where for each pair speed-steering, the resulting torque allocation can be easily obtained.

The results shown in Figure 9 can be justified considering the vertical load that the wheels receive in each scenario. The vertical load is related to the maximum torque that a wheel admits without sliding (Equation 25) and, since the objective is reducing the longitudinal slip, it is reasonable to assign a greater torque to those wheels receiving more vertical load.

Descriptively, the torque allocation strategy shows a tendency from equally distributed torque to rear axle torque allocation with speed as well as a transition from an evenly torque distribution to an outer-turn torque balancing with speed and steering angle.

5 Tests

The control strategy proposed above has been tested in simulation (using a more detailed FOX model presented in [18]) and on the real prototype. This Section presents the scenarios used in both cases.

The scenarios selected aim to register how the control behaves under different lateral acceleration conditions and for that, the steering angle and the speed have been varied from one test to another.

It has to be noticed that, since a symmetric behavior around the longitudinal axis is assumed, only left-hand turning are performed.

Simulation Tests

The simulation tests comprise a set of maneuvers to compare the longitudinal slip evolution obtained with an evenly torque distribution and the proposed control.

These scenarios correspond to a curve trajectory described at constant steering angle and at con-

ISBN 978-84-15914-12-9

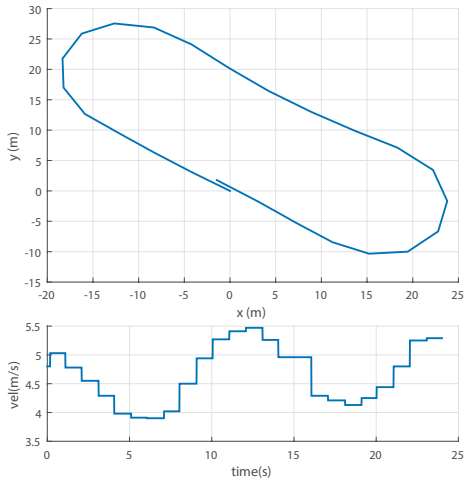

Figura 11: Real test: maneuver #1

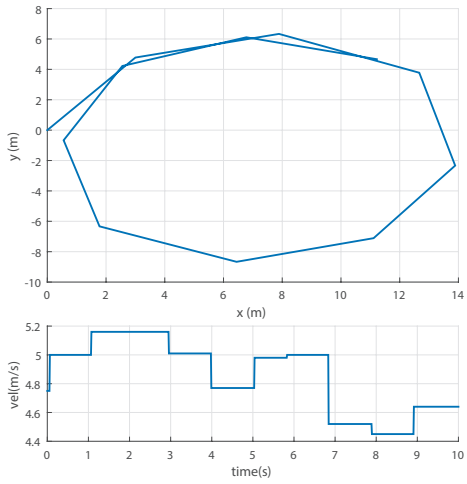

Figura 12: Real test: maneuver #2

stant speed as Figure 10 illustrates. The control performance is evaluated with the longitudinal slip reduction value measured during the simulation (Equation 37). Additionally, the difference with respect to the theoretical Ackerman radius is measured with Equation 38 to obtain further conclusions.

$$\mathrm{LS}_{\mathrm{Red}} = \overline{\mathrm{LS}}_{\mathrm{Evenly}} - \overline{\mathrm{LS}}_{\mathrm{Control}} \tag{37}$$

$$R_{\mathrm{Red}} = |R_{\mathrm{Evenly}} - R_{\mathrm{Ack}}| - |R_{\mathrm{Control}} - R_{\mathrm{Ack}}| \tag{38}$$

Real Tests

The strategy developed was also tested on the real car with the intention of proving its implementability as well as the performance reported in simulation. During the tests, two different maneuvers were described: on the one hand, a 180 degrees turning (e.g. Figure 11) with an approximately constant radius (around 8 m) with different speeds (as high as possible given the testing area), and on the other hand, a circular trajectory (e.g. Figure 12) described as fast as possible attempting to provoke a sliding.

It is worth stressing that, since the addressed control strategy changes the way in which the torque is distributed, the maneuvers should be described while some amount of torque is requested to notice the controller effect. Otherwise the vehicle behavior wouldn't depend on the control and no difference would be expected.

6 Results

This Section presents the most significant results extracted from the tests detailed in the previous Section.

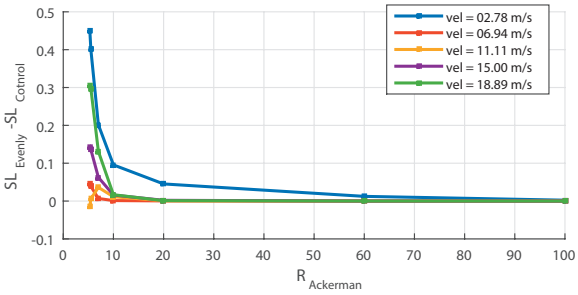

Figura 13: Longitudinal Slip Enhancing reported in simulations vs the theoretical Ackerman radius corresponding to the steering angle fixed.

6.1 Simulation Tests

Simulations report a longitudinal slip reduction in virtually all the cases tested. The slip reduction obtained in each case is shown in Figure 13 from where it is possible to observe the situations in which the control has a stronger influence. In particular, for those situation corresponding to high speeds and small radius trajectories, the control proposed presents a higher total longitudinal slip reduction in absolute terms.

Additionally, it can be observed that the final trajectory described by the vehicle is closer to the *ideal trajectory* given by the theoretical Ackerman radius. Figure 14 shows the radius reduction achieved in different conditions.

Real Tests

The analysis of the signals measured during the real tests presents some difficulties. On the one hand, the variable being optimized can't be measured directly from the real prototype. In consequence, the simulator has to be used to obtain it from the real input signals. On the other hand,

ISBN 978-84-15914-12-9

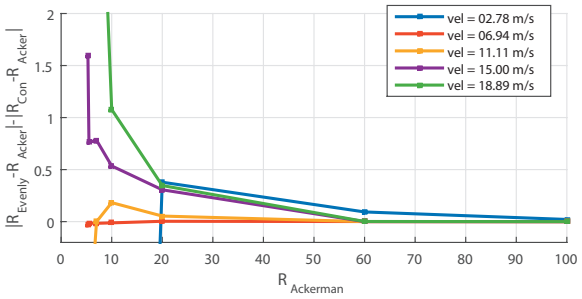

Figura 14: Trajectory's Radius Enhancing reported in simulations vs the theoretical Ackerman radius corresponding to the steering angle fixed.

in the same way that in the simulation tests, it would be desirable to apply exactly the same input signals two times: a first time with an evenly distributed torque applied and a second time with the control activated. However, it is virtually impossible to replicate the same input signals and the same external conditions from one test to another. For these reasons, the real tests analysis is done by applying the real speed and steering signals to the simulator, and carrying out one simulation for each torque allocation strategy.

Regarding the *numerical results*, figures 15 and 16 show two representative results extracted from a pair of simulations (one for the 180 degree turning case and the other for the circular trajectory case) carried out with the real input signals. It can be seen how the longitudinal slip ratio decreases during all the simulation, with the greatest diminutions taking place when the grater speed values are registered.

Furthermore, the driving feelings during the tests are the next: during 180 degrees turning situations, although a slight enhancing in terms of maneuverability in the control case was experienced, both strategies felt very similar as a consequence of the maximum speed limitation.

During the sliding test, since the trajectory radius reached was smaller, the difference was more noticeable and it was harder to do the vehicle slide with the control applied.

7 Conclusions

Torque distribution strategies, up to now, have been hardly tested on real sized prototypes, being based strictly on simulation results instead. Besides, almost all of them are on-line strategies which assume being able to measure accurately the value of specific variables in real time. Among them, lot of works assume having available the value of the slip, and others parameters whose values are enclosed to a high grade of uncertainty.

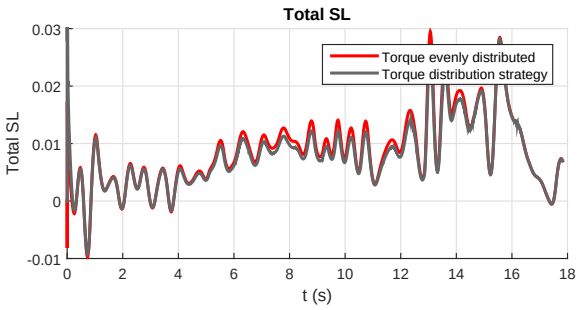

Figura 15: Real test #1. Total longitudinal slip in a 180 degree turning. Red: Torque evenly distributed, Gray: Torque distribution according to control

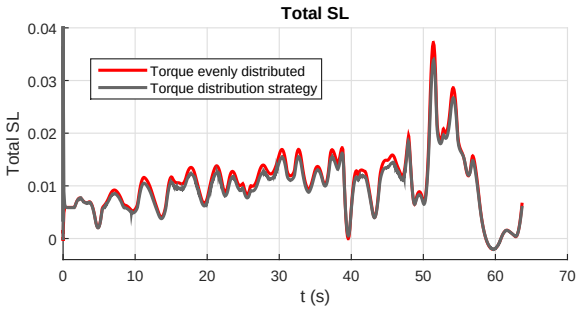

Figura 16: Real test data #2. Total longitudinal slip in a circular trajectory. Red: Torque evenly distributed, Gray: Torque distribution according to control

The approach here presented is simple-to-use while enhances the behavior experienced in terms of longitudinal slip. In contrast with other approaches, this strategy is designed and tuned off-line, what makes the strategy to be far from being optimal in some circumstances. Despite this, it always entails an improvement compared to an equally torque distribution configuration.

Acknowledgments

The authors gratefully acknowledge the Spanish Ministry of Economy and Competitiveness for its financial support of part of this work through the grant DPI2013-46912-C2-1.

Referencias

[1] ,Bosetti, Valentina and Longden, Thomas, Light duty vehicle transportation and global climate policy: The importance of electric drive vehicles, 2013, *Energy Policy vol 58 p. 209-219.*

[2] Burckhardt, Manfred, Fahrwerktechnik: Radschlupf-Regelsysteme, 1993, *Vogel-Verlag, Germany, p 16.*

ISBN 978-84-15914-12-9

[3] Chen, Yan and Wang, Junmin, Design and experimental evaluations on energy efficient control allocation methods for overactuated electric vehicles: Longitudinal motion case, 2014, *Mechatronics, IEEE/ASME Transactions on, p 538-548*

[4] De Novellis, Leonardo and Sorniotti, Aldo and Gruber, Patrick, Wheel Torque Distribution Criteria for Electric Vehicles With Torque-Vectoring Differentials, 2014, *Vehicular Technology, IEEE Transactions on. vol 63, p 1593-1602.*

[5] De Novellis, Leonardo and Sorniotti, Aldo and Gruber, Patrick, Optimal wheel torque distribution for a four-wheel-drive fully electric vehicle, 2013, *SAE Technical Paper.*

[6] Gerard, Mathieu and Verhaegen, Michel, Global and local chassis control based on load sensing, *American Control Conference, 2009. ACC'09 p 677-682.*

[7] Hawkins, Troy R and Gausen, Ola Moa and Strømman, Anders Hammer, Environmental impacts of hybrid and electric vehicles—a review, 2012, *The International Journal of Life Cycle Assessment, vol. 17, p. 997-1014.*

[8] Jonasson, Mats and Andreasson, Johan and Solyom, Stefan and Jacobson, Bengt and Trigell, Annika Stensson, Utilization of actuators to improve vehicle stability at the limit: From hydraulic brakes toward electric propulsion, 2011, *Journal of Dynamic Systems, Measurement, and Control, vol. 133, n 5.*

[9] Kenta Maeda, Horishi Fujimoto and Yoichi Hori Four-wheel Driving-force Distribution Method Based on Driving Stiffness and Slip Ratio Estimation for Electric Vehicle with In-wheel Motors, 2012, *IEEE Vehicle Power and Propulsion Conference, Oct 9-12, Seoul, Korea.*

[10] Kiencke, Uwe and Nielsen, Lars, Automotive control systems: for engine, driveline, and vehicle, 2000, *Measurement Science and Technology p 1828.*

[11] Macek, Kristijan and Thoma, Konrad and Glatzel, Richard and Siegwart, Roland, Dynamics modeling and parameter identification for autonomous vehicle navigation, *Intelligent robots and systems, 2007. IROS 2007. IEEE/RSJ international conference on.*

[12] Montero, Carlos and Marcos, David and Bordons, Carlos and Ridao, Miguel A and Camacho, EF and Gonzalez, Elena and Oliva, Alejandro, Modeling and torque control for a 4-wheel-drive electric vehicle, *Industrial Technology (ICIT), 2015 IEEE International Conference on.*

[13] Leonardo De Novellis, Member, Aldo Sorniotti, and Patrick Gruber, Wheel Torque Distribution Criteria for Electric Vehicles With Torque-Vectoring Differentials. 2014, *IEEE Transactions on vehicular technology, Vol. 63, NO. 4.*

[14] Lewis D, Naive (Bayes) at forty: the independence assupmtion in informaion retrieval. 1998.

[15] Rajamani, Rajesh, Vehicle dynamics and control, 2011, *Springer Science & Business Media*

[16] Uwe Kiencke and Lars Nielsen, Automotive Control Systems, 2005, *Springer-Verlag.*

[17] Wang, Junmin and Longoria, Raul G, Coordinated and reconfigurable vehicle dynamics control, *Control Systems Technology, IEEE Transactions on*, 2009, *IEEE.*

[18] Wideberg, Johan and Bordons, Carlos and Luque, Pablo and Mántaras, Daniel A and Marcos, David and Kanchwala, Husain, Development and Experimental Validation of a Dynamic Model for Electric Vehicle with in Hub Motors, *Procedia-Social and Behavioral Sciences, p 84-91*

[19] Yan Chen and Junmin Wang, Design and Evaluation on Electric Differentials for Overactuated Electric Ground Vehicles With Four Independent In-Wheel Motors, *IEEE Transactions on vehicular technology, vol. 61, NO. 4 May 2012.*